NeuroImage 281 (2023) 120382

Contents lists available at ScienceDirect

NeuroImage

journal homepage: www.elsevier.com/locate/ynimg

Functional ultrasound reveals effects of MRI acoustic noise on brain function

Keigo Hikishima [a,b,*], Tomokazu Tsurugizawa [c], Kazumi Kasahara [c], Ryusuke Hayashi [c], Ryo Takagi [a], Kiyoshi Yoshinaka [a], Naotaka Nitta [a]

[a] Health and Medical Research Institute, National Institute of Advanced Industrial Science and Technology (AIST), 1-2-1 Namiki, Tsukuba, Ibaraki 305-8564, Japan
[b] Okinawa Institute of Science and Technology Graduate University, 1919-1 Tancha, Onna-son, Okinwa 904-0495, Japan
[c] Human Informatics and Interaction Research Institute, National Institute of Advanced Industrial Science and Technology (AIST), 1-1-1 Higashi, Tsukuba 305-8568, Japan

ARTICLE INFO

Keywords:
Functional ultrasound
Functional MRI
Acoustic noise
Resting state
Functional connectivity
Brain activity

ABSTRACT

Loud acoustic noise from the scanner during functional magnetic resonance imaging (fMRI) can affect functional connectivity (FC) observed in the resting state, but the exact effect of the MRI acoustic noise on resting state FC is not well understood. Functional ultrasound (fUS) is a neuroimaging method that visualizes brain activity based on relative cerebral blood volume (rCBV), a similar neurovascular coupling response to that measured by fMRI, but without the audible acoustic noise. In this study, we investigated the effects of different acoustic noise levels (silent, 80 dB, and 110 dB) on FC by measuring resting state fUS (rsfUS) in awake mice in an environment similar to fMRI measurement. Then, we compared the results to those of resting state fMRI (rsfMRI) conducted using an 11.7 Tesla scanner. RsfUS experiments revealed a significant reduction in FC between the retrosplenial dysgranular and auditory cortexes (0.56 ± 0.07 at silence vs 0.05 ± 0.05 at 110 dB, p=.01) and a significant increase in FC anticorrelation between the infralimbic and motor cortexes (−0.21 ± 0.08 at silence vs −0.47 ± 0.04 at 110 dB, p=.017) as acoustic noise increased from silence to 80 dB and 110 dB, with increased consistency of FC patterns between rsfUS and rsfMRI being found with the louder noise conditions. Event-related auditory stimulation experiments using fUS showed strong positive rCBV changes (16.5% ± 2.9% at 110 dB) in the auditory cortex, and negative rCBV changes (−6.7% ± 0.8% at 110 dB) in the motor cortex, both being constituents of the brain network that was altered by the presence of acoustic noise in the resting state experiments. Anticorrelation between constituent brain regions of the default mode network (such as the infralimbic cortex) and those of task-positive sensorimotor networks (such as the motor cortex) is known to be an important feature of brain network antagonism, and has been studied as a biological marker of brain disfunction and disease. This study suggests that attention should be paid to the acoustic noise level when using rsfMRI to evaluate the anticorrelation between the default mode network and task-positive sensorimotor network.

1. Introduction

Functional ultrasound (fUS) imaging is a promising tool for visualizing brain activity at high spatiotemporal resolution through assessment of relative cerebral blood volume (rCBV) images (Mace et al., 2011). It has been used to investigate functional networks as well as rCBV signal changes coupled with neuronal activity (Bergel et al., 2018; Ferrier et al., 2020; Osmanski et al., 2014). fUS offers several features that make it attractive for the imaging of brain activity, such as high sensitivity (Deffieux et al., 2021), imaging of freely-moving rodents (Sieu et al., 2015; Tiran et al., 2017; Urban et al., 2015), and 4D imaging (Brunner et al., 2020; Rabut et al., 2019), and its use is rapidly increasing, with high clinical utility being suggested (Baranger et al., 2021; Soloukey et al., 2019).

An important feature of fUS is that the frequency of the emitted ultrasound is a few MHz, and therefore, unlike MRI, there is no acoustic noise in the audible range. This means that the localization of auditory-responsive regions in the cerebral cortex and deep brain areas, and their functional connectivity (FC), can be accurately mapped without interference from acoustic noise, offering potential as an auditory research

* Corresponding author at: 1-2-1 Namiki, Tsukuba, Ibaraki 305-8564, Japan.
E-mail address: k-hikishima@aist.go.jp (K. Hikishima).

https://doi.org/10.1016/j.neuroimage.2023.120382
Received 27 July 2023; Received in revised form 2 September 2023; Accepted 18 September 2023
Available online 19 September 2023

tool. Bimbard performed fUS in ferrets presented with sounds of different frequencies and reconstructed tonotopic maps of the auditory cortex, medial geniculate nucleus, and lateral lemniscus, which together compose the auditory pathway (Bimbard et al., 2018).

By comparison, when using functional MRI (fMRI), attention should be paid to the effects of acoustic noise on the results of fMRI experiments. Previous studies revealed that the presence of this acoustic noise during task-based fMRI affects the blood oxygenation level-dependent (BOLD) response, not only in the auditory cortex (Bandettini et al., 1998; Gaab et al., 2007), but also in several other regions such as the prefrontal cortex (Tomasi et al., 2005) and visual cortex (Zhang et al., 2005). It was also reported that in resting state fMRI (rsfMRI), differences in the level of acoustic noise affect the resting state FC between anatomically separated brain regions, including the default mode network (DMN), auditory network, and sensorimotor network (Andoh et al., 2017; Gaab et al., 2008; Langers and van Dijk, 2011; Rondinoni et al., 2013). However, the precise effects of loud acoustic noise on brain-wide activity are not known.

In this study, the effects of MRI acoustic noise on resting state FC were investigated using fUS by comparing it with fMRI. The acoustic noise level was set to 80 dB or 110 dB because the MRI acoustic noise generated by a typical MR sequence used for fMRI is generally within the range of 80–110 dB (Price et al., 2001). The target brain regions were part of the DMN, sensorimotor network, and auditory network, which are present in both mice and humans (Mandino et al., 2022; Sforazzini et al., 2014).

2. Materials and methods

2.1. Animals

A total of 20 male mice (C57Bl/6 J, CLEA Japan, Japan) were used in this study, 11 for fMRI experiments and 9 for fUS experiments. The sample sizes for fMRI and fUS experiments were determined according to previous studies (Ferrier et al., 2020; Osmanski et al., 2014; Tsurugizawa and Yoshimaru, 2021). fUS experiments, unlike fMRI experiments, require craniotomies, and obtaining a sufficient number of animals is not as easy as with MRI. Therefore, the number of samples used in this fUS experiment was smaller than in fMRI. All procedures were performed in accordance with the Laboratory Animal Welfare Act and the Guide for the Care and Use of Laboratory Animals (National Institutes of Health). The experimental protocols were reviewed by the Institutional Animal Care and Use Committees of the National Institute of Advanced Industrial Science and Technology of Japan (Approval No. 2020–0359) and the Okinawa Institute of Science and Technology Graduate University of Japan (Approval No. 2018–214) and approved. All mice were housed under a 12-hour light/dark cycle and had free access to food and water.

2.2. Surgery and habituation for awake imaging

In our previous functional brain network study, we found that resting state FC, calculated from synchronization of BOLD signal fluctuations between brain regions, was reduced by anesthesia not only in subcortical regions including insular cortex, thalamic nuclei, and parts of the limbic system, but also in a brain-wide area, including interhemispheric connectivity (Tsurugizawa and Yoshimaru, 2021). In this study, to investigate the effects of MRI acoustic noise on functional brain networks without the influence of anesthesia, we performed the following surgery and habituation training required for rsfMRI and rsfUS measurements in awake animals.

For the rsfMRI experiments using awake mice, we conducted the surgery for head bar implantation, following the methods of our previous study (Yoshida et al., 2016). The mice were anesthetized by subcutaneous injection of ketamine (75 mg/kg, Fujita, Japan) plus medetomidine (1.0 mg/kg, Kyoritsu Seiyaku, Japan) diluted in saline (0.9% NaCl). Heart and breathing rates were monitored, a rectal thermometer was inserted to monitor core body temperature, and a heating pad was placed under the animal during surgery to maintain the body temperature at 36.5 ± 0.5℃. The scalp was shaved and cleaned with povidone-iodine. The scalp was removed over the entire dorsal skull, and then the periosteum was also removed with a scalpel blade. Blood was carefully removed from the imaging area. Then, a head bar (20 × 3 × 2 mm) made of polyether ether ketone resin (PEEK), a non-metallic and strong resin that does not affect MRI measurements, was attached horizontally to the skull with dental cement (Super-Bond C&B, Sun Medical, Japan) in the flat skull position using a stereotaxic frame (SR-5M1-HT, Narishige, Japan). The head bar was positioned with the end of the bar 3 mm posterior to the bregma.

For the fUS experiments using awake mice, head plate implantation and craniotomy were performed following the method of a previous fUS study (Brunner et al., 2020), using the same anesthetic and vital control protocols as for the rsfMRI. The scalp was shaved and cleaned with povidone-iodine. The scalp was removed over the entire dorsal skull, and then the periosteum was also removed with a scalpel blade. A stainless-steel head plate with a large rectangular opening (13 × 11 mm) was attached to the skull with dental cement in the flat skull position. The head plate was positioned with the front end of the opening 5 mm anterior to the bregma. A craniotomy was performed with a dental drill using a 0.5 mm burr and the cranial window was protected when the mice were not being imaged. After surgery, mice were placed on a warm plate and monitored until awakening. Postoperative care included analgesics (buprenorphine, 0.1 mg/kg, NISSIN, Japan), antibiotics (cefazolin, 300 mg/kg, Nichiiko, Japan), and anti-inflammatory agents (dexamethasone, 0.5 mg/kg, Fuji Pharma, Japan). After recovery from the surgery, handling, and habituation to the head bar and plate holders and habituation training to MRI acoustic noise were performed following the method of our previous study (Tsurugizawa et al., 2021; Yoshida et al., 2016). First, the cupped hand method was used for the mice. Prior to habituation training, it was verified that the mice did not urinate and did not jump off the cupped hand during handling.

Then, the mice for rsfMRI and rsfUS measurements were fixed in a plastic head bar holder or metal head plate holder, respectively, and their bodies were placed on a plastic half-pipe (29 mm inner diameter). To minimize stress from the restraint, their bodies were gently wrapped in paper towels and absorbent pads were laid under the mice for urine absorption. Habituation to MRI acoustic noise was performed for 5 days in a soundproof box (O'Hara & Co., Japan) that mimicked the dark environment of an actual fMRI experiment, with MRI acoustic noise (110 dB, a spectrum with peaks in the range of 2–4 kHz; Supplementary Fig. 1) at a level equivalent to that measured at the center of the magnet bore during an rsfMRI experiment (Hamada, 2019).

2.3. Resting state fMRI acquisition

We scanned eleven mice using an 11.7-Tesla small animal MRI scanner (BioSpec117/11, Bruker Biospin GmbH, Germany) and a cryogenically-cooled RF coil (CryoProbe, Bruker Biospin AG, Switzerland). The imaging parameters included the following: gradient-echo-planar imaging; echo time (TE), 15 ms; repetition time (TR), 1500 ms; flip angle, 50°; number of averages, 1; spatial resolution, 0.2 × 0.2 × 0.5 mm; and 310 vol (acquisition time, 7.75 min). Two scans were acquired (one each in the anterior-posterior and left-right readout directions), and the left-right read out direction scans, which had relatively low distortion and ghost artifacts, were selected for analysis. For spatial normalization, a structural volume with the same field of view as the rsfMRI was acquired using a T2-weighted multi-slice rapid acquisition with relation enhancement (RARE) with the following parameters: TR, 2500 ms; effective TE, 20 ms; spatial resolution, 0.1 × 0.1 × 0.5 mm; RARE factor, 8; and two averages.

The animal handling and procedures used for rsfMRI measurements in awake mice, such as fixing the head bar to a plastic head bar holder

and holding the body to the bed, were the same as those used in the acclimation training for the awake measurements described earlier, and the measurement environment was shown in Fig. 1.

2.4. Functional US acquisition

The brain was covered by low-melting point 2% agarose (A9414, Sigma-Aldrich, USA) to reduce brain motion, and ultrasonic gel was placed on the agarose to ensure the proper acoustic coupling required for optimal transmission of the ultrasonic beam through the brain tissue. A high frequency linear array transducer (L22–14vX, Verasonics, USA) and a Vantage 128 ultrasound system (Verasonics, USA) controlled by a high-performance computing workstation equipped with four GPUs (AUTC, fUSI-2, Estonia) were used for the rCBV imaging. The L22–14vX transducer has 128 elements with a pitch of 0.1 mm and a center frequency of 18 MHz. High temporal resolution rCBV images at 10 Hz were acquired from awake mice in the soundproof box, mimicking the dark environment of the MRI experiment.

For the rsfUS experiments, six mice were scanned for 7.5 min each under three acoustic noise conditions (silence, 80 dB, or 110 dB). The silence consisted of the background noise intensity (40 dB) in the soundproof box.

For the event-related acoustic stimulation experiments, six mice (three of them also underwent the rsfUS experiment) were scanned, and each fUS trial consisted of a 15-s pre-stimulus baseline period followed by a 4-s stimulus of MRI acoustic noise (80 or 110 dB), and then a post-stimulus period for a total duration of 30 s. Ten trials were repeated for each stimulus.

The animal handling and procedures used for fUS measurements in awake mice, such as fixing the head plate to the head plate holder, holding the body to the bed, and soundproof box were the same as those used in the acclimation training for the awake resting state fMRI measurements described earlier, and the measurement environment was shown in Fig. 1.

2.5. Analysis of functional activity and resting state connectivity

The processing procedure for calculating FC from the rsfMRI and rsfUS signals is shown in Fig. 2.

For the preprocessing of rsfMRI data ($n = 11$) and rsfUS data ($n = 6$), SPM12 (Wellcome Trust Centre for Neuroimaging, UCL Institute of Neurology, London, UK) was used for motion correction with the default parameters (for rsfMRI data processing, the first 10 vol were discarded to account for non-steady state longitudinal magnetization, and adjustments for the timing of slice acquisition were applied prior to the motion correction). The voxel size was multiplied by 10 for use directly in SPM software. Framewise displacement (FD) was used to check head motion (Power et al., 2012), as shown in Supplementary Fig. 3. FD was calculated using six motion parameters (three for translation and three for rotation) from realignment, and the FD value was divided by 10 (because the pixel size was multiplied by 10 for analysis). The FD of the rsfMRI was comparable with that in our previous study (Tsurugizawa and Yoshimaru, 2021). For all animals, it was confirmed that the head motion was within the following criteria: (1) mean FD averaged over all time points of less than 0.03 mm; and (2) FD of less than 0.05 mm at all time points.

Next, to remove non-neural regions from the time series data, masks of the cerebral ventricles and large blood vessels were created using a k-means clustering filter in Advanced Normalization Tools software (ANTs) (Avants et al., 2011) applied to the time-averaged data, and these masks were applied to both the rsfMRI and rsfUS data. Next, to apply the same anatomical regions of interest (ROIs) to both rsfMRI and rsfUS data, all images were transformed to a C57Bl6 population-averaged stereotaxic brain template (https://www.nitrc.org/projects/tpm_mouse) (Hikishima et al., 2017) using ANTs.

Then, to remove movement artifacts from the temporal profile during scanning, the global change in the BOLD signals of rsfMRI or rCBV signals of rsfUS of the brain in each slice were regressed out (Ferrier et al., 2020) in the respective rsfMRI and rsfUS experiments.

Finally, low-frequency fluctuations (LFF) of rsfMRI and rsfUS signals were extracted using a bandpass filter (0.01–0.08 Hz) and the FC between brain regions were calculated from the extracted LFF with MATLAB version 2023a (The Mathworks, USA). The frequency range of the bandpass filter was based on parameters used in previous mouse studies and our experiments (Sforazzini et al., 2014; Tsurugizawa and Yoshimaru, 2021). FC is analyzed as the statistical dependence of LFF between brain regions. Various methods have been proposed for its analysis, including the Pearson correlation coefficient, which assumes linearity of activity between brain regions, and mutual Information and transfer entropy, which can analyze nonlinear dependence (Wang et al., 2014). For the FC analysis of fMRI and fUS in this study, we used the Pearson correlation coefficient, which is statistically easy to interpret and the most widely used method. The Pearson correlation analysis was applied to the time series data (7.5minutes, 300 points for rsfMRI and 4500 points for rsfUS) to calculate correlations between brain regions using anatomical ROIs at +1.5 mm and −3 mm slices from the bregma, according to the Paxinos atlas (Paxinos and Franklin, 2019).

In the event-related fUS analysis of the mice subjected to the acoustic noise stimulus, group-averaged ($n = 6$) correlation maps were generated by calculating the Pearson correlation coefficients between the rCBV

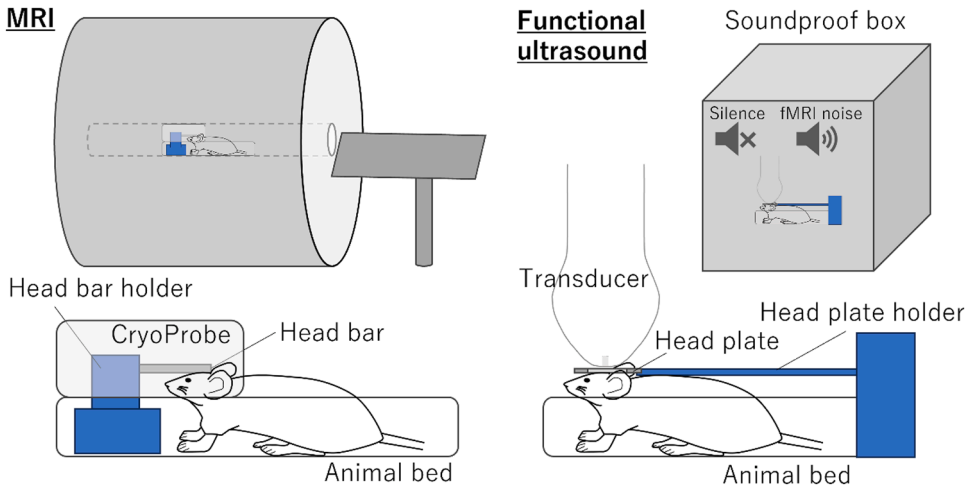

Fig. 1. Schematic of the experimental setup for awake fMRI and awake fUS.

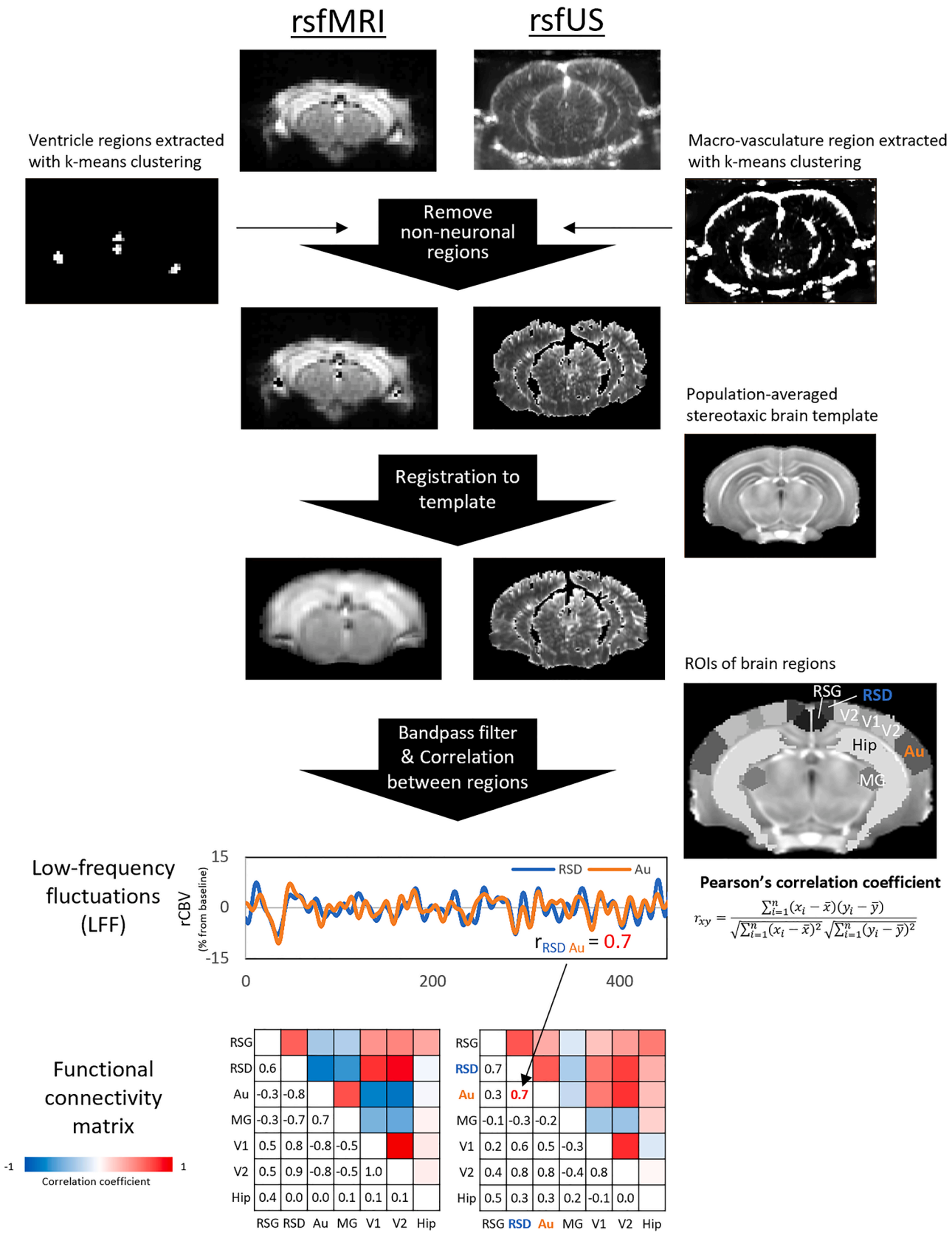

Fig. 2. Overview of resting state brain functional connectivity analysis applied to rsfMRI and rsfUS datasets. For the resting state functional MRI (rsfMRI) and resting state functional ultrasound (rsfUS) data, the non-neural components of the ventricles and macro-vasculature regions were removed with a k-means clustering filter, the images were registered to a population-averaged stereotaxic brain template, and after bandpass filtering, the synchronization of LFF between brain regions was evaluated using the Pearson correlation coefficient. Abbreviations: RSG, retrosplenial granular cortex; RSD, retrosplenial dysgranular cortex; Au, auditory cortex; MG, medial geniculate nucleus; V1, primary visual cortex; V2, secondary visual cortex; Hip, hippocampus.

signal changes and the square-wave pattern of the stimulus. Those voxels with correlation coefficients exceeding a threshold of ±0.1 and forming a cluster larger than four voxels were displayed on the population-averaged stereotaxic brain template. The temporal profiles of the rCBV changes in the auditory and primary motor (M1) cortexes were extracted from each mouse and were temporally smoothed with a 1.5 s moving average time window to reduce high-frequency fluctuations before group averaging.

2.6. Statistical analysis

Differences in the FC matrices between the three acoustic conditions (silence, 80 dB, or 110 dB) and differences in the FC matrices between rsfUS and rsfMRI were quantified using Cohen's d effect size estimates. Changes in FC between silence, 80 dB, and 110 dB were evaluated using *t*-tests with Bonferroni correction of significance thresholds for multiple comparisons, performed using SPSS Statistics version 28.0.1.0 (IBM,

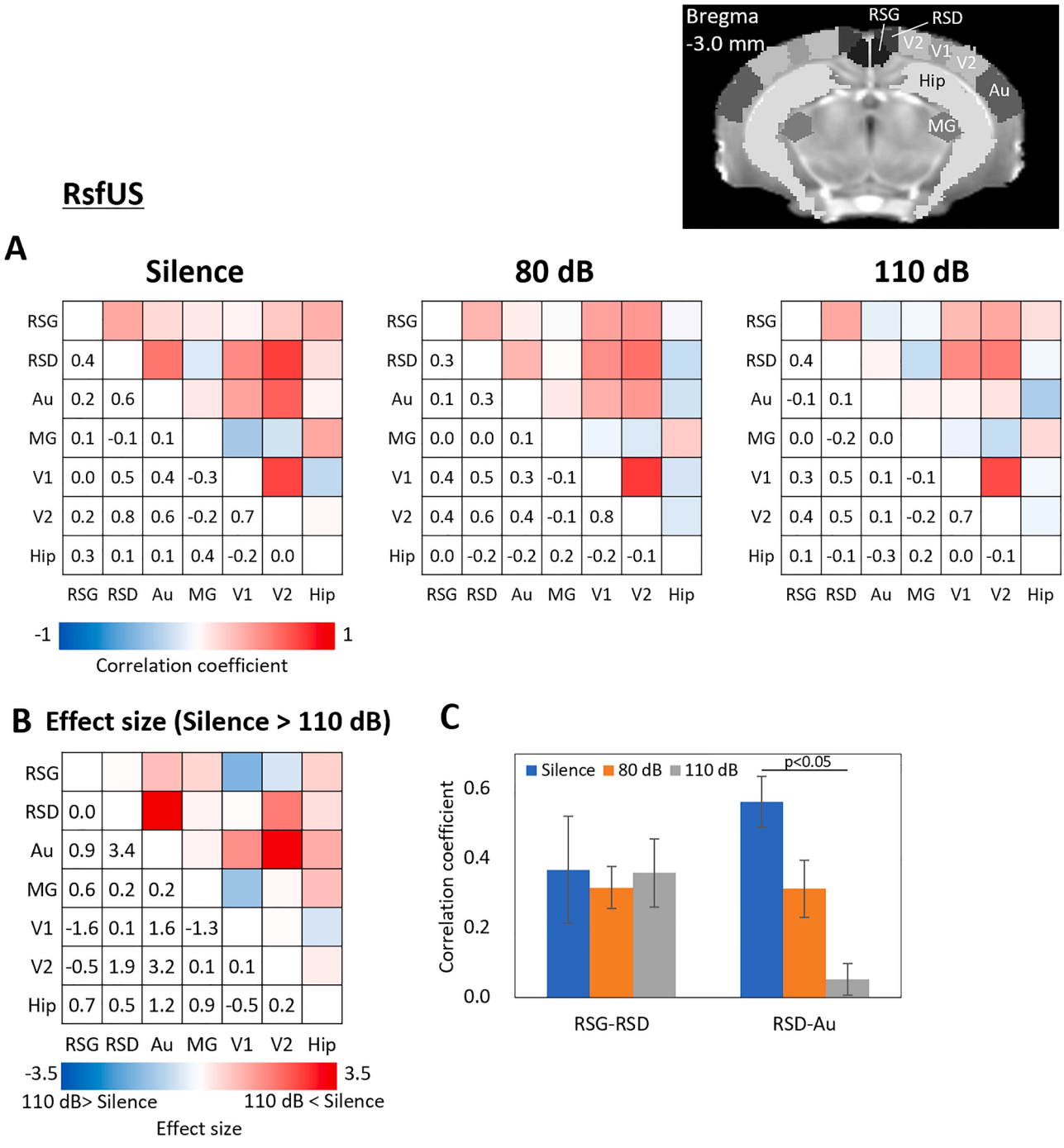

Fig. 3. Resting state FC changes measured by functional US under MRI acoustic noise within an image slice including the auditory cortex. A, Resting state functional connectivity (FC) matrices showing Pearson correlation coefficients between brain regions within a slice at −3 mm from the bregma (silence, 80 dB, or 110 dB of acoustic noise, averaged over $n = 6$). B, Cohen's d matrix showing the effect size used to indicate the standardized difference between the FC matrices of silence and 110 dB. The hot color in the matrix shows that the FC was higher at silence than at 110 dB, while the cold color shows that the FC at 110 dB was higher than at silence. C, Resting state FC under the three acoustic noise conditions of silence, 80 dB, and 110 dB for RSD-auditory and RSG-RSD connectivity. Abbreviations: rsfUS, resting state functional ultrasound; RSG, retrosplenial granular cortex; RSD, retrosplenial dysgranular cortex; Au, auditory cortex; MG, medial geniculate nucleus; V1, primary visual cortex; V2, secondary visual cortex; Hip, hippocampus.

USA).

3. Results

3.1. MRI acoustic noise caused reduced functional connectivity in auditory networks

First, we investigated how MRI acoustic noise modulates the auditory network, brain regions for which previous studies have reported the effects of acoustic noise on FC in the resting state. The MRI acoustic noise was applied throughout the rsfUS acquisition. At 110 dB of acoustic noise, FC with the auditory cortex was substantially reduced in many brain regions (effect size >0.9) compared with silence, except for connectivity with the medial geniculate (MG) nucleus (auditory thalamic relay nucleus) (Fig. 3). Among the regions analyzed, the reduction in FC between the retrosplenial dysgranular cortex (RSD; the core of the DMN) and the auditory cortex was most pronounced (effect size 3.4), as shown in Fig. 3B. By contrast, FC between the retrosplenial granular cortex (RSG)-RSD network, which is a part of the DMN, was not affected by 110 dB (effect size 0.0). We examined changes in FC between RSD-auditory and RSG-RSD at two different acoustic noise levels and found that the FC correlation coefficient for RSG-RSD did not change with greater sound level (0.37 ± 0.15 at silence vs 0.36 ± 0.10 at 110 dB, p=.99, uncorrected), whereas the RSD-auditory FC showed a lower correlation coefficient with greater sound level (0.56 ± 0.07 at silence vs 0.05 ± 0.05 at 110 dB, p=.01, Bonferroni corrected; Fig. 3C).

Next, we investigated the difference between the results of rsfUS under MRI acoustic noise and results obtained from actual rsfMRI (Fig. 4A), and found that the rsfUS-measured FC for RSD-auditory cortex became more similar to the rsfMRI results at greater sound levels (Fig. 4B).

For the whole FC matrix, the difference in the global effect size decreased from 0.86 to 0.69 with greater sound level, showing that although the FC measured by rsfUS was still significantly different from that measured by rsfMRI, the rsfUS-measured FC obtained with a similar acoustic noise level to the fMRI (110 dB) was more similar to the rsfMRI-measured FC (Fig. 4C).

3.2. Positive hemodynamic response in the auditory cortex elicited by MRI acoustic noise

For further confirmation, we additionally investigated the direct effects of MRI acoustic noise by performing an event-related fUS experiment with acoustic noise stimulation (4-s stimulus duration) in the same slice as the RSD-auditory network, a brain network that was altered by the presence of acoustic noises in the resting state experiments. Fig. 5A shows the averaged correlation maps between the rCBV changes and the stimulus square-wave pattern in a slice including the auditory cortex. Increased rCBV was observed in the bilateral auditory cortex and the MG of the thalamus during both 80 and 110 dB stimulation. The correlation coefficient in the auditory cortex with a 110 dB stimulus was greater than that with an 80 dB stimulus. We then extracted temporal changes in rCBV from an ROI of the auditory cortex (Fig. 5B). The peak percent changes in rCBV signal compared with the pre-stimulation baseline were 11.7% ± 2.1% (mean ± standard error of the peak values in each animal) at 80 dB and 22.0% ± 0.8% at 110 dB, respectively. The peak percent change at 110 dB was significantly higher than that at 80 dB (p=.027). The time-to-peak from stimulus onset was 3.0 ± 0.4 s at 80 dB and 2.4 ± 0.2 s at 110 dB. These results demonstrate that fUS is very sensitive to brain activity elicited by MRI acoustic noise and that the peak of rCBV change in the auditory cortex depended on the sound pressure level.

3.3. Anticorrelation between the DMN and motor cortex caused by MRI acoustic noise

Finally, as in the experiments on the auditory network, we examined how the MRI acoustic noise modulated the motor network in the resting state (Fig. 6). The largest differences in FC between brain regions at silence and 110 dB in rsfUS experiments were found between the infralimbic cortex (IL) and M1 (effect size 1.6), which is a part of the connections in the DMN and sensorimotor network (Fig. 6B). By contrast, the smallest difference in resting state FC was between the IL and the prelimbic cortex (PrL), which is an intra-DMN connection (effect size 0.0). We examined the changes in resting state FC between the above two brain connections (IL-M1 and IL-PrL) at two different acoustic noise levels and found that the correlation coefficient between IL and PrL did not show significant change with greater sound level (0.47 ± 0.06 at silence vs 0.47 ± 0.13 at 110 dB, p=.99 uncorrected), whereas the resting state FC between IL and M1 changed from a weak to moderate negative correlation (−0.21 ± 0.08 at silence vs −0.47 ± 0.04 at 110 dB, p=.017), as shown in Fig. 6C.

We further investigated the difference between rsfUS measured under the MRI acoustic noise environment and the actual rsfMRI (Fig. 7), and found that the FC between IL and M1 calculated from rsfUS became more similar to the rsfMRI results with greater sound level (Fig. 7B). For the FC matrix, the difference in the global effect size was not changed significantly, although the effect size gradually decreased with greater sound level (effect size of 1.29, 1.25, and 1.23 at silence, 80 dB, and 110 dB, respectively; Fig. 7C).

3.4. Negative hemodynamic response in the motor cortex elicited by MRI acoustic noise

For further confirmation, we additionally investigated the direct effects of MRI acoustic noise by performing an event-related fUS experiment with acoustic noise stimulation (4-s stimulus duration) in the same slice as the IL-M1 network, a brain network that was altered by the presence of acoustic noise in the resting state experiments.

Fig. 8A shows the averaged correlation maps with the stimulus in a slice including M1. Lower rCBV was observed in the bilateral M1 for both 80 and 110 dB conditions, and the hemodynamic response at 110 dB was widely decreased in M1 in comparison with 80 dB (Fig. 8A). The averaged rCBV change extracted from an M1 ROI at 110 dB showed a robust negative peak of −6.7% ± 0.8% at a time of 2.7 ± 0.1 s from stimulus onset, while the averaged rCBV change in M1 during 80 dB acoustic stimulation was not statistically significant.

4. Discussion

The present study demonstrated alterations in two fUS measures of brain activity under MRI acoustic noise; one was altered resting state FC, and the other was a hemodynamic response to MRI acoustic stimuli. Event-related fUS experiments with an MRI acoustic noise stimulus revealed a robust negative hemodynamic response in the motor cortex, in addition to a strong positive hemodynamic response in the auditory cortex. Greater acoustic noise levels induced widespread decreases in resting state FC with the auditory cortex and with the motor cortex, respectively, and anticorrelation between the DMN and motor cortex. FC measured by rsfUS became more similar to that measured by rsfMRI as the MRI acoustic noise level increased from silence to 80 dB and 110 dB (i.e., the loudness of the noise in rsfUS experiments approached that of the actual noise during rsfMRI, indicating that the MRI acoustic noise level modulates resting state FC).

4.1. MRI acoustic noise reduces resting state FC

Echo-planar imaging, a high-speed sequence used in fMRI measurements, generates extremely loud acoustic noise levels of about 110 dB

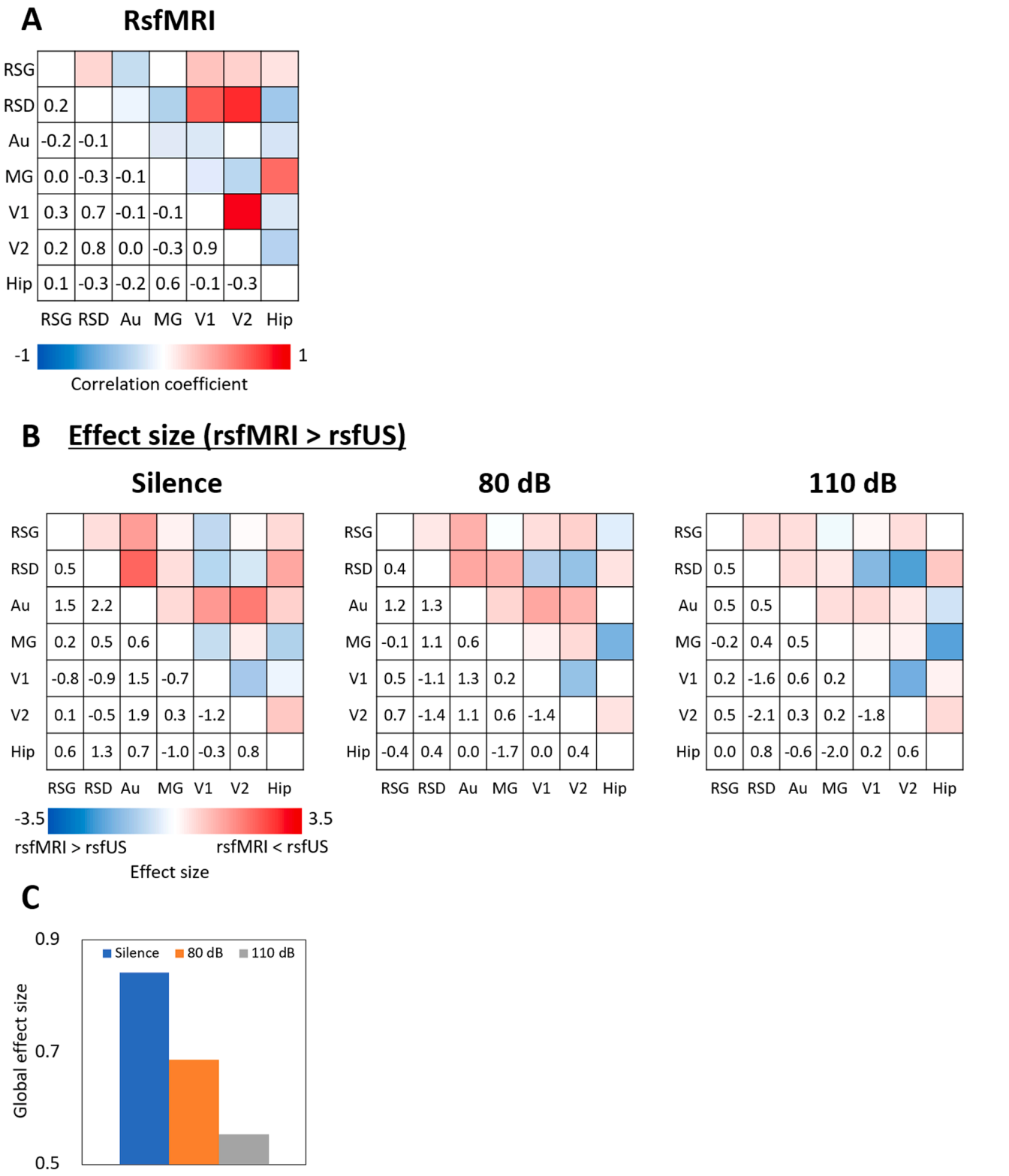

Fig. 4. Resting state functional MRI (rsfMRI)-measured FC within a slice including the auditory cortex. A, Resting state functional connectivity (FC) matrix showing the Pearson correlation coefficients between brain regions within a slice at −3 mm from the bregma, as measured by rsfMRI (averaged over $n = 11$). B, Cohen's d matrices showing the effect size used to indicate the standardized difference between the resting state FC matrices of fMRI and functional US (fUS) (silence, 80 dB, or 110 dB). Hot color in the matrix shows that the FC by rsfUS is higher than that by rsfMRI, while cold color shows that the FC by rsfMRI is higher than that by rsfUS. C, Global effect size within the Cohens's D matrix of (B) under the three acoustic noise conditions (silence, 80 dB, and 110 dB).

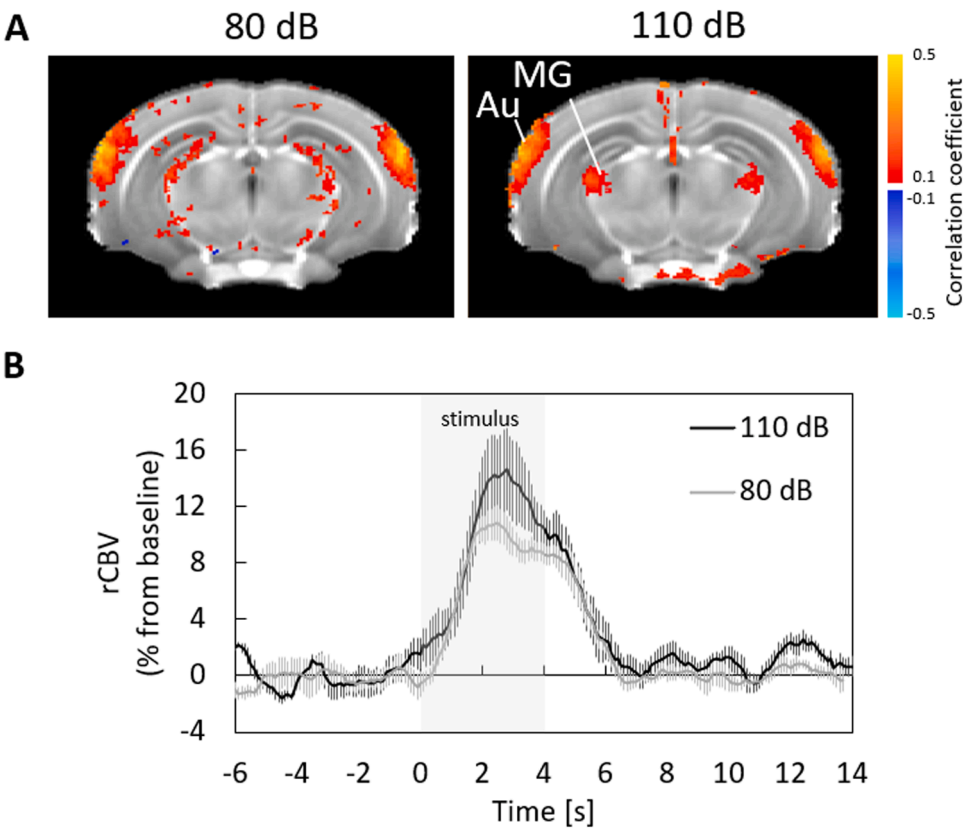

Fig. 5. Functional US (fUS)-measured positive rCBV changes in the auditory cortex elicited by the MRI acoustic noise stimulation. A, Correlation coefficient map showing correlations between rCBV changes and the square-wave pattern of the stimulation at −3 mm from the bregma (acoustic noise level of 80 or 110 dB, averaged over $n = 6$). Those voxels with correlation coefficients exceeding a threshold of ±0.1 and forming a cluster larger than four voxels were displayed on the population-averaged stereotaxic brain template. B, Averaged rCBV change in the auditory cortex region of interest (mean ± standard error, $n = 6$). Abbreviations: rCBV, relative cerebral blood volume; Au, auditory cortex; MG, medial geniculate nucleus.

due to the Lorentz forces acting on the gradient coils during the rapid switching of the magnetic gradient field used for image readout (Counter et al., 1997). Soundproofing devices such as headphones can reduce the acoustic noise level to about 80 dB, but it is still loud. To study auditory function with fMRI, a sparse temporal sampling method (Hall et al., 1999) was developed to reduce acoustic noise effects. This involved using a long repetition time and presenting the auditory task during a non-scanning period, and then measuring the hemodynamic response immediately after the auditory task. To investigate the effects of MRI acoustic noise on resting state brain activity, a relatively low acoustic noise level sequence based on the sparse temporal sampling method was compared to a normal sequence, and it was reported that the normal sequence resulted in weak FC in auditory and motor networks (Andoh et al., 2017). More recently, taking advantage of the quietness of magnetoencephalography, MRI acoustic noise was shown to decrease resting state FC in broad cortical regions connected to the auditory network and sensorimotor network (Pellegrino et al., 2022b). The reduction in FC measured by magnetoencephalography in the auditory network and sensorimotor network is not specific to MRI acoustic noise, but was also reported to occur with exposure to white noise (Pinardi et al., 2023), which is defined as a random acoustic signal with a flat spectral density.

In this study, rsfUS measurement under a greater acoustic noise condition resulted in lower FC in the auditory and motor networks, indicating that we may have captured the same biological phenomenon caused by MRI acoustic noise as that found in previous studies, although the functional contrast mechanism used in our experiment was rCBV changes measured by fUS, rather than BOLD signal changes measured by fMRI or alpha band changes on magnetoencephalography.

Even when loud acoustic noise is continuously present during scanning, as in fMRI, it is thought that the acoustic noise elevates the BOLD baseline in the auditory cortex (Hall et al., 1999). Although the reduction of resting state FC in the auditory network is thought to be due to the direct influence of acoustic noise on auditory functions, the reasons for the reduction in FC in non-auditory networks are not well understood.

4.2. *Negative hemodynamic response in M1 due to MRI acoustic noise*

Sound is known to be processed in various brain regions depending on the individual, the type of sound, and the situation (Lima et al., 2016; Medalla and Barbas, 2014; Rauschecker, 2018). It was also reported that providing white noise at some loud volume produces excitatory activity in the motor cortex and improves sensorimotor performance (Pellegrino et al., 2022a). Conversely, several groups reported that M1 activity was suppressed by loud sounds (Furubayashi et al., 2000; Kuhn et al., 2004). This suppression of M1 by loud sound has been found to be induced only in a resting state and not during voluntary muscle contraction of the upper arm (Chen et al., 2016). The suppression of M1 activity is thought to be partly mediated via ascending polysynaptic reticulocortical pathways, but little is known about this phenomenon (Kuhn et al., 2004).

The decreased rCBV in M1 elicited by loud acoustic noise stimuli in this study may capture the same suppression of M1 activity as that reported in previous studies using loud sound. Negative rCBV change was not only detected in M1 but also extended to regions in the sensorimotor network. Negative rCBV changes and suppression of neural activity shown by fUS have been discussed previously. Urban et al. reported that fUS imaging of rats undergoing forepaw electrical stimulation under

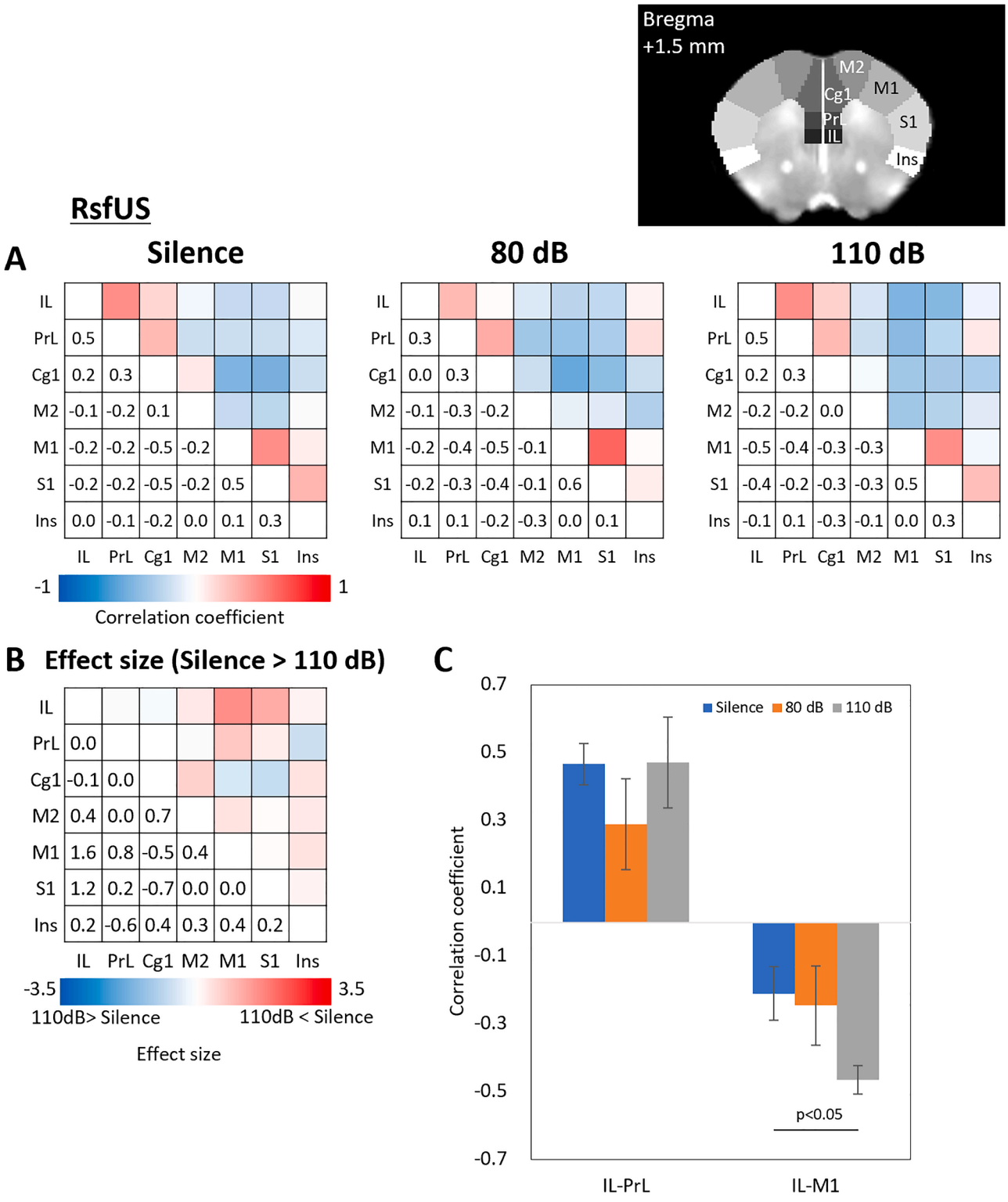

Fig. 6. Resting state functional US (rsfUS)-measured FC changes under MRI acoustic noise within a slice including the primary motor cortex. A, Resting state functional connectivity (FC) matrices showing the Pearson correlation coefficients between brain regions within a slice at +1.5 mm from the bregma (silence, 80 dB, or 110 dB MRI acoustic noise level, averaged over $n = 6$). B, Cohen's d matrix showing the effect size used to indicate the standardized difference between the resting state FC matrices for silence and 110 dB. The hot color in the matrix shows that the FC was higher at silence than at 110 dB, while the cold color shows that the FC was higher at 110 dB than at silence. C, Resting state FC under the three acoustic noise conditions of silence, 80 dB, and 110 dB in the IL-M1 and IL-PrL connections. Abbreviations: IL, infralimbic cortex; PrL, prelimbic cortex; Cg1, cingulate cortex area 1; M1, primary motor cortex; M2, secondary motor cortex; S1, somatosensory cortex; Ins, insular cortex.

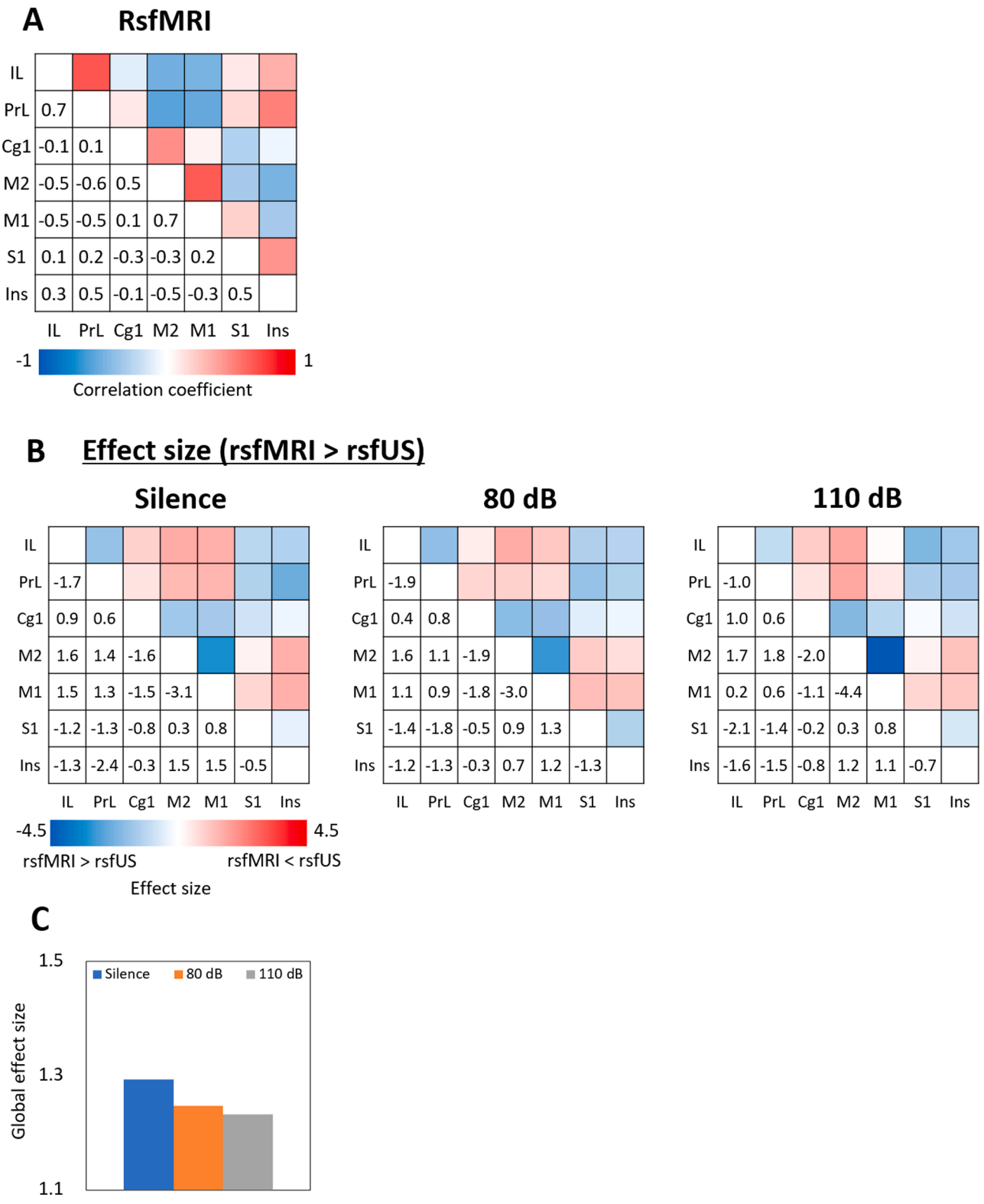

Fig. 7. Resting state functional MRI (fMRI)-measured FC within a slice including the primary motor cortex. A, Resting state functional connectivity (FC) matrix showing the Pearson correlation coefficients between brain regions within a slice at +1.5 mm from the bregma, as measured by rsfMRI (averaged over $n = 11$). B, Cohen's d matrix showing the effect size used to indicate the standardized difference between the FC matrices of rsfMRI and rsfUS (silence, 80 dB, or 110 dB). Hot color in the matrix shows that the FC by rsfUS is higher than that by rsfMRI, while cold color shows that the FC by rsfMRI is higher than that by rsfUS. C, Global effect size within the Cohens's D matrix from (B) under the three acoustic noise conditions (silence, 80 dB, or 110 dB).

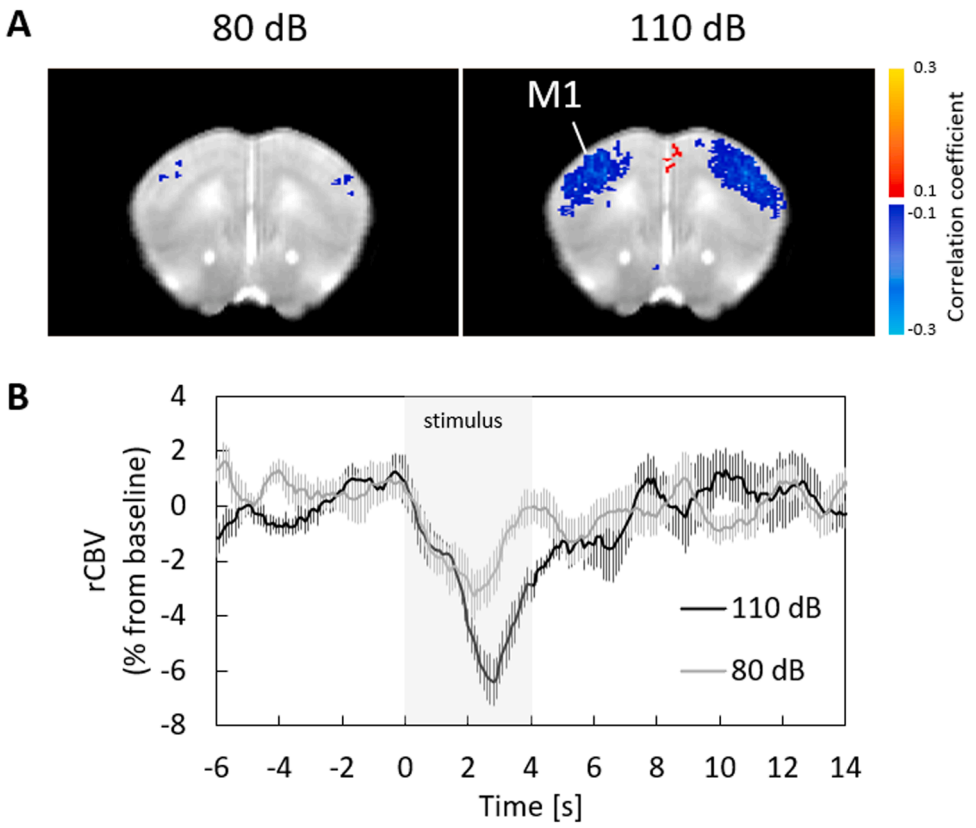

Fig. 8. Functional US (fUS)-measured negative rCBV changes in the primary motor cortex elicited by the MRI acoustic noise stimulus. A, Map of the correlation coefficients between rCBV changes and the stimulus pattern at +1.5 mm from the bregma (acoustic noise levels of 80 and 110 dB, averaged over $n = 6$). Those voxels with correlation coefficients exceeding a threshold of ±0.1 and forming a cluster larger than four voxels were displayed on the population-averaged stereotaxic brain template. B, Averaged rCBV change in the M1 region of interest (mean ± standard error, $n = 6$). Abbreviations: rCBV, relative cerebral blood volume; M1, primary motor cortex.

ketamine/ xylazine anesthesia detected positive rCBV changes of around 20% in the contralateral forelimb somatosensory cortex (S1FL), whereas negative rCBV changes of around −5% were detected in the ipsilateral S1FL, with these being thought to be due to interhemispheric suppression (Urban et al., 2014).

4.3. Anticorrelation between the DMN and motor cortex

The discovery of resting state functional networks began with the reporting of the sensorimotor network by Biswal (Biswal et al., 1995). The sensorimotor network, a part of the task-positive network (TPN) responsible for somatosensory and motor control that is activated during motor tasks, is similar in rodents, monkeys, and humans (Schwarz et al., 2013; Sierakowiak et al., 2015).

The DMN, which is active at rest and inactive during cognitive tasks, was reported by Raichle (Raichle et al., 2001). It is temporally anticorrelated with TPNs such as the sensorimotor network, with this anticorrelation between the networks reflecting the antagonistic state between the DMN and TPNs (Fox et al., 2005). This anticorrelation is an important feature of resting state networks because it is closely related to brain functional dynamics.

It was reported that the anticorrelation between the sensorimotor network (one of the TPNs targeted by this study) and the DMN is weaker in older than in younger people (Rodriguez-Sabate et al., 2019). Furthermore, the higher the clinical dementia scale in Alzheimer's disease, the weaker the anticorrelation (Brier et al., 2012), implying that the DMN-TPN anticorrelation can be a potential biological disease marker.

Valchev reported that continuous theta burst stimulation to the somatosensory cortex delivered by transcranial magnetic stimulation, which suppressed neural activity during rsfMRI acquisition, resulted in reduced FC in the somatosensory cortex (Valchev et al., 2015).

We thus hypothesize that MRI acoustic noise exogenously affects the weak endogenous DMN-sensorimotor network anticorrelation, changing it to moderate anticorrelation. When the subject's sensitivity to sound differs from normal level (e.g., because of age-related hearing loss, dementia, or hearing hypersensitivity), modulation of the antagonistic state between the DMN and sensorimotor network during fMRI scanning could possibly differ from that of subjects with a normal hearing level because of the MRI acoustic noise. Future validation is needed to clarify this, such as research using MRI acoustic noise conditions with fUS in animal models of auditory disease. Future experiments using functional near infra-red spectroscopy (fNIRS) to validate the results of this study in humans may also advance our understanding of the effects of MRI acoustic noise on functional brain networks. Functional NIRS, despite its limited spatial resolution and measurement depth, can observe changes in the concentration of oxygenated and deoxygenated hemoglobin, providing a contrast similar to BOLD in fMRI (Pellegrino et al., 2016), and also allowing evaluation of resting state functional connectivity (Zhang et al., 2010). Furthermore, fNIRS causes no acoustic noise during the measurement and the small size of the device makes it easy to control the measurement environment and the posture of the examinee. Therefore, measurements under MRI noise and silence conditions can be performed with that the subject in the same posture as in MRI experiments.

4.4. Limitations

Our study has some limitations. We used MRI acoustic noise that consisted of a wide continuous frequency range with a peak between 2

and 4 kHz, rather than a specific frequency. Therefore, it is unclear which frequency range of sound affected resting state FC in this study. Further experiments under various conditions, such as using a pure tone or combinations of sounds with multiple frequencies as a stimulus, could be considered to address the remaining questions. However, these questions are beyond the scope of this study.

Another limitation is that fUS is invasive because of the craniotomy required for widespread imaging of deep brain. Furthermore, ultrasound has difficulty penetrating past the anterior temporal bone, which is difficult to remove by craniotomy, and there was signal loss in the surrounding brain area in our fUS experiments. In our fMRI experiments, some auditory cortex images showed distortion and signal loss due to magnetic susceptibility effects from air in the ear canal (Supplementary Fig. 3). These modality-specific artifacts may reduce the accuracy of resting state FC analysis. However, fMRI can also measure resting state FC by obtaining rCBV measurements using blood-pool superparamagnetic iron oxide (SPIO) (Sforazzini et al., 2014). This method makes it possible to compare fMRI and fUS through a more similar functional contrast. Therefore, we consider that it would be interesting future work to investigate whether rCBV-based rsfMRI and rsfUS under acoustic noise show the same FC patterns as shown in the present study.

5. Conclusions

The functional US measurements made under MRI acoustic noise clearly showed that the resting state functional connectivity of the auditory network was suppressed and that the anticorrelation between the default mode network and motor network was strengthened. These findings suggest that attention should be paid to acoustic noise levels when assessing those networks using rsfMRI. These findings also highlight the advantage of using fUS to investigate functional connectivity across extensive brain regions under various sound conditions, a measurement challenge typically encountered in fMRI studies.

Data and code availability statement

The data supporting the reported findings are available from the corresponding author upon reasonable request.

CRediT authorship contribution statement

Keigo Hikishima: Conceptualization, Methodology, Software, Validation, Formal analysis, Writing – original draft, Writing – review & editing, Visualization, Supervision, Funding acquisition. **Tomokazu Tsurugizawa:** Conceptualization, Methodology, Software, Investigation, Writing – original draft, Writing – review & editing. **Kazumi Kasahara:** Conceptualization, Methodology, Software, Validation, Formal analysis, Investigation, Writing – original draft, Writing – review & editing. **Ryusuke Hayashi:** Resources, Writing – review & editing. **Ryo Takagi:** Conceptualization, Methodology, Resources, Writing – review & editing. **Kiyoshi Yoshinaka:** Conceptualization, Methodology, Resources, Writing – review & editing, Funding acquisition. **Naotaka Nitta:** Conceptualization, Methodology, Resources, Writing – review & editing.

Declaration of Competing Interest

The authors declare no competing interests.

Acknowledgments

A part of this work was carried out by AMED under Grant Numbers (JP20he0422004j0001 and JP22ym0126803j0001) to K.H., by a Grant-in-Aid for Scientific Research (21K19749) to K.H., by a Grant for Basic Science Research Projects from The Sumitomo Foundation (200372) to K.H., and by a grant for promoting public utilization of advanced research infrastructure (JPMXS0450400422) funded by the JST/MEXT, Japan.

Supplementary materials

Supplementary material associated with this article can be found, in the online version, at doi:10.1016/j.neuroimage.2023.120382.

References

Andoh, J., Ferreira, M., Leppert, I.R., Matsushita, R., Pike, B., Zatorre, R.J., 2017. How restful is it with all that noise? Comparison of Interleaved silent steady state (ISSS) and conventional imaging in resting-state fMRI. Neuroimage 147, 726–735.
Avants, B.B., Tustison, N.J., Song, G., Cook, P.A., Klein, A., Gee, J.C., 2011. A reproducible evaluation of ANTs similarity metric performance in brain image registration. Neuroimage 54, 2033–2044.
Bandettini, P.A., Jesmanowicz, A., Van Kylen, J., Birn, R.M., Hyde, J.S., 1998. Functional MRI of brain activation induced by scanner acoustic noise. Magn. Reson. Med. 39, 410–416.
Baranger, J., Demene, C., Frerot, A., Faure, F., Delanoe, C., Serroune, H., Houdouin, A., Mairesse, J., Biran, V., Baud, O., Tanter, M., 2021. Bedside functional monitoring of the dynamic brain connectivity in human neonates. Nat. Commun. 12, 1080.
Bergel, A., Deffieux, T., Demene, C., Tanter, M., Cohen, I., 2018. Local hippocampal fast gamma rhythms precede brain-wide hyperemic patterns during spontaneous rodent REM sleep. Nat. Commun. 9, 5364.
Bimbard, C., Demene, C., Girard, C., Radtke-Schuller, S., Shamma, S., Tanter, M., Boubenec, Y., 2018. Multi-scale mapping along the auditory hierarchy using high-resolution functional ultrasound in the awake ferret. eLife 7.
Biswal, B., Yetkin, F.Z., Haughton, V.M., Hyde, J.S., 1995. Functional connectivity in the motor cortex of resting human brain using echo-planar MRI. Magn. Reson. Med. 34, 537–541.
Brier, M.R., Thomas, J.B., Snyder, A.Z., Benzinger, T.L., Zhang, D., Raichle, M.E., Holtzman, D.M., Morris, J.C., Ances, B.M., 2012. Loss of intranetwork and internetwork resting state functional connections with Alzheimer's disease progression. J. Neurosci. 32, 8890–8899.
Brunner, C., Grillet, M., Sans-Dublanc, A., Farrow, K., Lambert, T., Mace, E., Montaldo, G., Urban, A., 2020. A platform for brain-wide volumetric functional ultrasound imaging and analysis of circuit dynamics in awake mice. Neuron 108, 861–875 e867.
Chen, Y.T., Li, S., Zhou, P., Li, S., 2016. Different Effects of startling acoustic stimuli (SAS) on TMS-induced responses at rest and during sustained voluntary contraction. Front. Hum. Neurosci. 10, 396.
Counter, S.A., Olofsson, A., Grahn, H.F., Borg, E., 1997. MRI acoustic noise: sound pressure and frequency analysis. J. Magn. Reson. Imaging 7, 606–611.
Deffieux, T., Demene, C., Tanter, M., 2021. Functional ultrasound imaging: a new imaging modality for neuroscience. Neuroscience 474, 110–121.
Ferrier, J., Tiran, E., Deffieux, T., Tanter, M., Lenkei, Z., 2020. Functional imaging evidence for task-induced deactivation and disconnection of a major default mode network hub in the mouse brain. Proc. Natl. Acad. Sci. USA 117, 15270–15280.
Fox, M.D., Snyder, A.Z., Vincent, J.L., Corbetta, M., Van Essen, D.C., Raichle, M.E., 2005. The human brain is intrinsically organized into dynamic, anticorrelated functional networks. Proc. Natl. Acad. Sci. USA 102, 9673–9678.
Furubayashi, T., Ugawa, Y., Terao, Y., Hanajima, R., Sakai, K., Machii, K., Mochizuki, H., Shiio, Y., Uesugi, H., Enomoto, H., Kanazawa, I., 2000. The human hand motor area is transiently suppressed by an unexpected auditory stimulus. Clin. Neurophysiol. 111, 178–183.
Gaab, N., Gabrieli, J.D., Glover, G.H., 2007. Assessing the influence of scanner background noise on auditory processing. I. An fMRI study comparing three experimental designs with varying degrees of scanner noise. Hum. Brain Mapp. 28, 703–720.
Gaab, N., Gabrieli, J.D., Glover, G.H., 2008. Resting in peace or noise: scanner background noise suppresses default-mode network. Hum. Brain Mapp. 29, 858–867.
Hall, D.A., Haggard, M.P., Akeroyd, M.A., Palmer, A.R., Summerfield, A.Q., Elliott, M.R., Gurney, E.M., Bowtell, R.W., 1999. Sparse" temporal sampling in auditory fMRI. Hum. Brain Mapp. 7, 213–223.
Hamada, H., 2019. Serotonergic Control of Brain-Wide Dynamics. Okinawa Institute of Science and Technology Graduate University.
Hikishima, K., Komaki, Y., Seki, F., Ohnishi, Y., Okano, H.J., Okano, H., 2017. In vivo microscopic voxel-based morphometry with a brain template to characterize strain-specific structures in the mouse brain. Sci. Rep. 7, 85.
Kuhn, A.A., Sharott, A., Trottenberg, T., Kupsch, A., Brown, P., 2004. Motor cortex inhibition induced by acoustic stimulation. Exp. Brain Res. 158, 120–124.
Langers, D.R., van Dijk, P., 2011. Robustness of intrinsic connectivity networks in the human brain to the presence of acoustic scanner noise. Neuroimage 55, 1617–1632.
Lima, C.F., Krishnan, S., Scott, S.K., 2016. Roles of supplementary motor areas in auditory processing and auditory imagery. Trends Neurosci. 39, 527–542.
Mace, E., Montaldo, G., Cohen, I., Baulac, M., Fink, M., Tanter, M., 2011. Functional ultrasound imaging of the brain. Nat. Methods 8, 662–664.
Mandino, F., Vrooman, R.M., Foo, H.E., Yeow, L.Y., Bolton, T.A.W., Salvan, P., Teoh, C. L., Lee, C.Y., Beauchamp, A., Luo, S., Bi, R., Zhang, J., Lim, G.H.T., Low, N., Sallet, J., Gigg, J., Lerch, J.P., Mars, R.B., Olivo, M., Fu, Y., Grandjean, J., 2022. A triple-network organization for the mouse brain. Mol. Psychiatry 27, 865–872.

Medalla, M., Barbas, H., 2014. Specialized prefrontal "auditory fields": organization of primate prefrontal-temporal pathways. Front. Neurosci. 8, 77.
Osmanski, B.F., Pezet, S., Ricobaraza, A., Lenkei, Z., Tanter, M., 2014. Functional ultrasound imaging of intrinsic connectivity in the living rat brain with high spatiotemporal resolution. Nat. Commun. 5, 5023.
Paxinos, G., Franklin, K.B., 2019. Paxinos and Franklin's the Mouse Brain in Stereotaxic Coordinates. Academic press.
Pellegrino, G., Machado, A., von Ellenrieder, N., Watanabe, S., Hall, J.A., Lina, J.M., Kobayashi, E., Grova, C., 2016. Hemodynamic response to interictal epileptiform discharges addressed by personalized EEG-fNIRS recordings. Front. Neurosci. 10, 102.
Pellegrino, G., Pinardi, M., Schuler, A.L., Kobayashi, E., Masiero, S., Marioni, G., di Lazzaro, V., Keller, F., Arcara, G., Piccione, F., Di Pino, G., 2022a. Stimulation with acoustic white noise enhances motor excitability and sensorimotor integration. Sci. Rep. 12, 13108.
Pellegrino, G., Schuler, A.L., Arcara, G., Di Pino, G., Piccione, F., Kobayashi, E., 2022b. Resting state network connectivity is attenuated by fMRI acoustic noise. Neuroimage 247, 118791.
Pinardi, M., Schuler, A.L., Arcara, G., Ferreri, F., Marinazzo, D., Di Pino, G., Pellegrino, G., 2023. Reduced connectivity of primary auditory and motor cortices during exposure to auditory white noise. Neurosci. Lett. 804, 137212.
Power, J.D., Barnes, K.A., Snyder, A.Z., Schlaggar, B.L., Petersen, S.E., 2012. Spurious but systematic correlations in functional connectivity MRI networks arise from subject motion. Neuroimage 59, 2142–2154.
Price, D.L., De Wilde, J.P., Papadaki, A.M., Curran, J.S., Kitney, R.I., 2001. Investigation of acoustic noise on 15 MRI scanners from 0.2 T to 3 T. J. Magn. Reson. Imaging 13, 288–293.
Rabut, C., Correia, M., Finel, V., Pezet, S., Pernot, M., Deffieux, T., Tanter, M., 2019. 4D functional ultrasound imaging of whole-brain activity in rodents. Nat. Methods 16, 994–997.
Raichle, M.E., MacLeod, A.M., Snyder, A.Z., Powers, W.J., Gusnard, D.A., Shulman, G.L., 2001. A default mode of brain function. Proc. Natl. Acad. Sci. USA 98, 676–682.
Rauschecker, J.P., 2018. Where, when, and how: are they all sensorimotor? Towards a unified view of the dorsal pathway in vision and audition. Cortex 98, 262–268.
Rodriguez-Sabate, C., Morales, I., Sanchez, A., Rodriguez, M., 2019. The functional interaction of the brain default network with motor networks is modified by aging. Behav. Brain Res. 372, 112048.
Rondinoni, C., Amaro Jr., E., Cendes, F., dos Santos, A.C., Salmon, C.E., 2013. Effect of scanner acoustic background noise on strict resting-state fMRI. Braz. J. Med. Biol. Res. 46, 359–367.
Schwarz, A.J., Gass, N., Sartorius, A., Risterucci, C., Spedding, M., Schenker, E., Meyer-Lindenberg, A., Weber-Fahr, W., 2013. Anti-correlated cortical networks of intrinsic connectivity in the rat brain. Brain Connect 3, 503–511.
Sforazzini, F., Schwarz, A.J., Galbusera, A., Bifone, A., Gozzi, A., 2014. Distributed BOLD and CBV-weighted resting-state networks in the mouse brain. Neuroimage 87, 403–415.
Sierakowiak, A., Monnot, C., Aski, S.N., Uppman, M., Li, T.Q., Damberg, P., Brene, S., 2015. Default mode network, motor network, dorsal and ventral basal ganglia networks in the rat brain: comparison to human networks using resting state-fMRI. PLoS One 10, e0120345.
Sieu, L.A., Bergel, A., Tiran, E., Deffieux, T., Pernot, M., Gennisson, J.L., Tanter, M., Cohen, I., 2015. EEG and functional ultrasound imaging in mobile rats. Nat. Methods 12, 831–834.
Soloukey, S., Vincent, A., Satoer, D.D., Mastik, F., Smits, M., Dirven, C.M.F., Strydis, C., Bosch, J.G., van der Steen, A.F.W., De Zeeuw, C.I., Koekkoek, S.K.E., Kruizinga, P., 2019. Functional ultrasound (fUS) during awake brain surgery: the clinical potential of intra-operative functional and vascular brain mapping. Front. Neurosci. 13, 1384.
Tiran, E., Ferrier, J., Deffieux, T., Gennisson, J.L., Pezet, S., Lenkei, Z., Tanter, M., 2017. Transcranial functional ultrasound imaging in freely moving awake mice and anesthetized young rats without contrast agent. Ultrasound Med. Biol. 43, 1679–1689.
Tomasi, D., Caparelli, E.C., Chang, L., Ernst, T., 2005. fMRI-acoustic noise alters brain activation during working memory tasks. Neuroimage 27, 377–386.
Tsurugizawa, T., Tamada, K., Debacker, C., Zalesky, A., Takumi, T., 2021. Cranioplastic surgery and acclimation training for awake mouse fMRI. Bio. Protoc. 11, e3972.
Tsurugizawa, T., Yoshimaru, D., 2021. Impact of anesthesia on static and dynamic functional connectivity in mice. Neuroimage 241, 118413.
Urban, A., Dussaux, C., Martel, G., Brunner, C., Mace, E., Montaldo, G., 2015. Real-time imaging of brain activity in freely moving rats using functional ultrasound. Nat. Methods 12, 873–878.
Urban, A., Mace, E., Brunner, C., Heidmann, M., Rossier, J., Montaldo, G., 2014. Chronic assessment of cerebral hemodynamics during rat forepaw electrical stimulation using functional ultrasound imaging. Neuroimage 101, 138–149.
Valchev, N., Curcic-Blake, B., Renken, R.J., Avenanti, A., Keysers, C., Gazzola, V., Maurits, N.M., 2015. cTBS delivered to the left somatosensory cortex changes its functional connectivity during rest. Neuroimage 114, 386–397.
Wang, H.E., Benar, C.G., Quilichini, P.P., Friston, K.J., Jirsa, V.K., Bernard, C., 2014. A systematic framework for functional connectivity measures. Front. Neurosci. 8, 405.
Yoshida, K., Mimura, Y., Ishihara, R., Nishida, H., Komaki, Y., Minakuchi, T., Tsurugizawa, T., Mimura, M., Okano, H., Tanaka, K.F., Takata, N., 2016. Physiological effects of a habituation procedure for functional MRI in awake mice using a cryogenic radiofrequency probe. J. Neurosci. Methods 274, 38–48.
Zhang, H., Zhang, Y.J., Lu, C.M., Ma, S.Y., Zang, Y.F., Zhu, C.Z., 2010. Functional connectivity as revealed by independent component analysis of resting-state fNIRS measurements. Neuroimage 51, 1150–1161.
Zhang, N., Zhu, X.H., Chen, W., 2005. Influence of gradient acoustic noise on fMRI response in the human visual cortex. Magn. Reson. Med. 54, 258–263.